Circular and linear magnetic birefringences in xenon at λ=1064 nm

Cadene, Agathe; Fouche, Mathilde; Rivere, Alice; Battesti, Remy; Coriani, Sonia; Rizzo, Antonio; Rizzo, Carlo

Published in:
Journal of Chemical Physics

Link to article, DOI:
10.1063/1.4916049

Publication date:
2015

Document Version
Publisher's PDF, also known as Version of record

AIP | The Journal of Chemical Physics

Circular and linear magnetic birefringences in xenon at λ = 1064 nm

Agathe Cadène, Mathilde Fouché, Alice Rivère, Rémy Battesti, Sonia Coriani, Antonio Rizzo, and Carlo Rizzo

Citation: The Journal of Chemical Physics **142**, 124313 (2015); doi: 10.1063/1.4916049
View online: http://dx.doi.org/10.1063/1.4916049
View Table of Contents: http://scitation.aip.org/content/aip/journal/jcp/142/12?ver=pdfcov
Published by the AIP Publishing

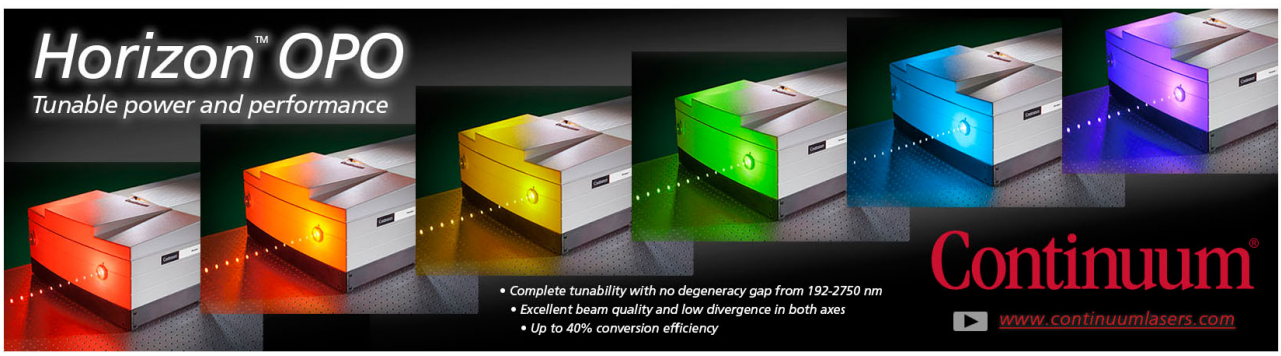

Circular and linear magnetic birefringences in xenon at λ = 1064 nm

Agathe Cadène,[1] Mathilde Fouché,[1] Alice Rivère,[1] Rémy Battesti,[1] Sonia Coriani,[2,3] Antonio Rizzo,[4] and Carlo Rizzo[1,a)]

[1]*Laboratoire National des Champs Magnétiques Intenses (UPR 3228, CNRS-UPS-UJF-INSA), 143 Avenue de Rangueil, 31400 Toulouse, France*
[2]*Dipartimento di Scienze Chimiche e Farmaceutiche, Università degli Studi di Trieste, via Giorgieri 1, 34127 Trieste, Italy*
[3]*Aarhus Institute of Advanced Studies, Aarhus University, DK-8000 Aarhus C, Denmark*
[4]*Istituto per i Processi Chimico-Fisici del Consiglio Nazionale delle Ricerche (IPCF-CNR), Area della Ricerca, via G. Moruzzi 1, I-56124 Pisa, Italy*

(Received 19 January 2015; accepted 11 March 2015; published online 30 March 2015)

The circular and linear magnetic birefringences corresponding to the Faraday and the Cotton-Mouton effects, respectively, have been measured in xenon at λ = 1064 nm. The experimental setup is based on time dependent magnetic fields and a high finesse Fabry-Pérot cavity. Our value of the Faraday effect is the first measurement at this wavelength. It is compared to theoretical predictions. Our uncertainty of a few percent yields an agreement at better than 1σ with the computational estimate when relativistic effects are taken into account. Concerning the Cotton-Mouton effect, our measurement, the second ever published at λ = 1064 nm, agrees at better than 1σ with theoretical predictions. We also compare our error budget with that established for other experimental published values. © *2015 AIP Publishing LLC.* [http://dx.doi.org/10.1063/1.4916049]

I. INTRODUCTION

Magnetic birefringence corresponds to an anisotropy of the (generally complex) refractive index induced in a medium by a magnetic field.[1,2] A circular birefringence arises when the magnetic field changes the angular velocity of the two eigen modes of polarization in which a linearly polarized beam is split, without deforming them. The net result is a rotation of the plane of linear polarization, a phenomenon also seen in the absence of external fields in chiral samples (natural optical rotation). When the presence of the external magnetic field yields a different phase of two perpendicular components of the linear polarization vector, the net result is the appearance of an ellipticity, and we are observing an example of linear birefringence.

Two well known examples of magnetic birefringences are the Faraday and the Cotton-Mouton effects. The former corresponds to a circular birefringence induced by a longitudinal magnetic field $B_\parallel$ (aligned parallel to the direction of propagation of light). After going through the birefringent medium, the real part of the index of refraction for left circularly polarized light n_- is different from that for right circularly polarized light n_+. The difference $\Delta n_F = n_- - n_+$ is proportional to $B_\parallel$,

$$\Delta n_F = k_F B_\parallel, \tag{1}$$

k_F being the circular magnetic birefringence per unit magnetic field intensity. For historical reason, the Faraday effect is usually given in terms of the Verdet constant,

$$V = \frac{\pi k_F}{\lambda}, \tag{2}$$

where λ is the light wavelength. On the other hand, the Cotton-Mouton effect corresponds to a linear magnetic birefringence induced by a transverse magnetic field $B_\perp$. The field induces a difference between the real parts of the refraction index for light polarized parallel $n_\parallel$ with respect to that polarized perpendicular to the magnetic field $n_\perp$. The difference $\Delta n_{CM} = n_\parallel - n_\perp$ is proportional to the square of the magnetic field,

$$\Delta n_{CM} = k_{CM} B_\perp^2, \tag{3}$$

with k_{CM} the linear magnetic birefringence per square unit magnetic field intensity.

For the Cotton-Mouton effect, k_{CM} has two contributions, the first one due to the distortion of the electronic structure while the second one corresponds to a partial orientation of the molecules. When working in the conditions of constant volume, the orientational contribution is proportional to the inverse of the temperature T, and it usually dominates, often hiding the first temperature independent contribution. For axial molecules, for example, k_{CM} is given by the expression[3]

$$k_{CM} = \frac{\pi N_A}{V_m 4\pi\epsilon_0}\left(\Delta\eta + \frac{2}{15 k_B T}\Delta\alpha\Delta\chi\right). \tag{4}$$

Above N_A is the Avogadro constant, V_m the molar volume, k_B the Boltzmann constant, ϵ_0 the electric constant, $\Delta\eta$ the frequency dependent hypermagnetizability anisotropy, $\Delta\alpha$ the optical electric dipole polarizability anisotropy, and $\Delta\chi$ the magnetic susceptibility anisotropy. For spherical molecules or for atoms, such as xenon, however, the temperature dependent contribution vanishes. Measurements on noble gases, for example, allow to focus on the hypermagnetizability anisotropy $\Delta\eta$ term. On the other hand, since the Langevin-type orientational term vanishes, the magnetic birefringence is much lower than the one observed in nonspherical molecules.

a)Electronic mail: carlo.rizzo@lncmi.cnrs.fr

From an experimental point of view, measurements on such gases require a very sensitive apparatus, with a Δn_{CM} of the order of 10^{-16} for helium and 10^{-14} for xenon at 1 atm and with a magnetic field of 1 T. In comparison, Δn_F is typically 10^5 bigger.

The computational determination of the Verdet constant and of the Cotton-Mouton effect requires the far-from-trivial calculation of higher-order response functions,[2,3] and it has often served as a test bed for the validation of new electronic structure methods. For atoms, in order to obtain accurate results, one must properly account for the appropriate description of one-electron (basis set), N-electron (correlation), and relativistic effects. As far as correlation is concerned, coupled cluster (CC) methods are nowadays among the most accurate tools in electronic structure theory.[4,5] Both birefringences treated here, and in particular, the Cotton-Mouton effect, require a good description of the outer valence space of the system at hand. Therefore, the presence of diffuse functions in the one-electron basis set is mandatory.[2,4] Whereas for light atoms, relativistic corrections are minor, their importance increases and they become significant for heavier atoms. For example, Ekström *et al.*[6] have calculated that for helium, the relativistic effects add −0.03% to the non-relativistic Verdet value. For xenon, the heaviest non-radioactive noble atom, relativistic corrections add 3%–4%, depending on the chosen wavelength. In this case, relativistic effects cannot be ignored in accurate calculations.

In this article, we report both measurements and calculations of Faraday and Cotton-Mouton effects at $\lambda = 1064$ nm. We perform the first measurement of the Faraday effect of xenon at this wavelength, and our estimate bears an uncertainty of a few percent. Concerning the Cotton-Mouton effect, our measurement, the second ever published at $\lambda = 1064$ nm, agrees at better than 1σ with theoretical predictions and we also compare our error budget with that established for other experimental published values. Our theoretical predictions, that can be considered of state-of-the-art quality, were obtained at the coupled cluster singles and doubles (CCSD)[7–9] and coupled cluster singles, doubles and approximate triples (CC3)[10–13] levels of theory, and they include estimates of relativistic effects. For both effects, our theoretical predictions are within 1σ of our experimental data.

II. EXPERIMENTAL SETUP

A. Principle of the measurement

Experimentally, we determine the Faraday and the Cotton-Mouton effects by measuring, respectively, the rotation induced by a longitudinal magnetic field and the ellipticity induced by a transverse magnetic field on an incident linear polarization. For small angles, the induced rotation θ_F depends on the circular birefringence as follows:

$$\theta_F = \pi \frac{L_B}{\lambda} \Delta n_F, \tag{5}$$

where L_B is the length of the magnetic field region. The induced ellipticity ψ_{CM} is related to the linear birefringence by the formula,

$$\psi_{CM} = \pi \frac{L_B}{\lambda} \Delta n_{CM} \sin 2\theta_P, \tag{6}$$

where θ_P is the angle between the light polarization and the magnetic field.

B. General setup

The apparatus has already been described in detail elsewhere.[14,15] Briefly, light comes from a Nd:YAG laser at $\lambda = 1064$ nm (see Fig. 1). It is linearly polarized by a first polarizer P, before going through either a transverse or a longitudinal magnetic field. The polarization is then analyzed by a second polarizer A, crossed at maximum extinction compared to P. The beam polarized parallel to the incident beam, reflected by the polarizer A as the ordinary ray, is collected by the photodiode Ph_t. Its power is denoted by I_t. The beam polarized perpendicular to the incident beam (power I_e), corresponding to the extraordinary ray that passes through the polarizer A, is collected by the low noise and high gain photodiode Ph_e.

This setup has been designed to measure the linear magnetic birefringence of vacuum[16] and its sensitivity allows to perform precise measurements on gases.[15,17] All the optical components from A to P are placed in an ultrahigh-vacuum chamber. To perform birefringence measurement on gases, we fill the vacuum chamber with a high-purity gas. For this particular measurement, we have used a bottle of xenon with a global purity higher than 99.998%.

C. Fabry-Pérot cavity

Magnetic birefringence measurements on dilute gases are difficult, especially at low pressure, because one has to detect very small variations of light polarization. To increase the measured signal, one needs high magnetic fields. One also needs an as large as possible path length in the field L_B (cf. Eqs. (5) and (6)). To this end, optical cavities are used to trap light in the magnetic field region and therefore enhance the signal to be measured.

As shown in Fig. 1, the cavity is formed by two mirrors M_1 and M_2, placed at both sides of the magnetic field region. The laser frequency is locked to the cavity resonance frequency, using the Pound-Drever-Hall technique.[18] The electro-optic modulator generates 10 MHz sidebands, and the signal reflected by the cavity is detected by the photodiode Ph_r. The laser frequency is adjusted with the acousto-optic modulator, the piezoelectric, and the Peltier elements of the laser.

This cavity increases the distance traveled by light in the magnetic field by a factor $2F/\pi$, where F is the cavity finesse. Therefore, the rotation induced by the longitudinal magnetic field becomes

$$\Theta_F(t) = \frac{2F}{\pi} \theta_F(t), \tag{7}$$

with θ_F the rotation acquired without any cavity. In the same way, the ellipticity induced by the transverse magnetic field

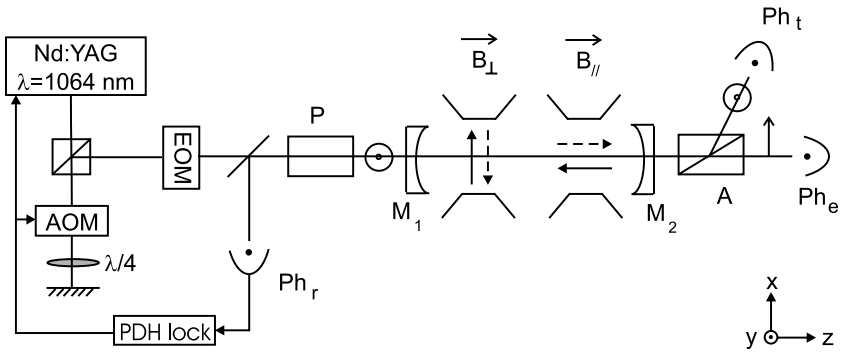

FIG. 1. Experimental setup. EOM = electro-optic modulator; AOM = acousto-optic modulator; PDH = Pound-Drever-Hall; Ph = photodiode; P = polarizer; and A = analyzer. See text for more details.

becomes

$$\Psi_{\mathrm{CM}}(t) = \frac{2F}{\pi}\psi_{\mathrm{CM}}(t), \tag{8}$$

with ψ_{CM} denoting the ellipticity acquired without any cavity. The cavity finesse is inferred from the measurement of the photon lifetime τ inside the cavity,[19]

$$F = 2\pi\Delta^{\mathrm{FSR}}\tau, \tag{9}$$

with Δ^{FSR} as the cavity free spectral range. For the Faraday effect, the cavity finesse was about $F = 475\,000$. For the Cotton-Mouton effect, two sets of mirrors were used with a respective finesse of about 400 000 and 480 000.

D. Raw signals

We measure the circular and the linear magnetic birefringence by measuring the ratio $I_{\mathrm{e}}/I_{\mathrm{t}}$,

$$\frac{I_{\mathrm{e}}(t)}{I_{\mathrm{t,f}}(t)} = \sigma^2 + [\Gamma + \Psi_{\mathrm{CM}}(t)]^2 + [\epsilon + \Theta_{\mathrm{F}}(t)]^2. \tag{10}$$

As said previously, I_{e} (I_{t}) corresponds to the power of light polarized perpendicular (parallel) to the incident beam. The subscript f indicates that we need to take into account the cavity filtering, as explained in detail in the previous papers.[15,19] The term σ^2 corresponds to the extinction ratio of polarizers P and A, Γ is the total static ellipticity due to the cavity mirrors, and ϵ is the static angle between the major axis of the elliptical polarization and the incident polarization. The extinction ratio and the static birefringence are measured before each magnetic pulse. The static angle ϵ can be estimated but its value is not needed for the analysis.

III. CIRCULAR MAGNETIC BIREFRINGENCE

A. Magnetic field

The magnetic field is generated by a solenoid previously used for Faraday effect measurement in helium.[15] Its characteristics have already been explained in detail.[15] Here, we just briefly recall its main features. It generates a longitudinal magnetic field with an equivalent length $L_B = (0.308 \pm 0.006)$ m at 1σ. This magnetic field is modulated at the frequency ν = 18 Hz: $B_{\parallel} = B_{\parallel,0}\sin(2\pi\nu t + \phi)$. The rotation of the polarization due to the Faraday effect is thus given by

$$\Theta_{\mathrm{F}} = \Theta_0 \sin(2\pi\nu t + \phi), \tag{11}$$

$$\text{with } \Theta_0 = \frac{2F}{\pi} V B_{\parallel,0} L_B. \tag{12}$$

B. Data analysis

Expanding Eq. (10), the raw signal becomes

$$\frac{I_{\mathrm{e}}(t)}{I_{\mathrm{t,f}}(t)} = \sigma^2 + \Gamma^2 + \epsilon^2 + 2\epsilon\Theta_{\mathrm{F}}(t) + \Theta_{\mathrm{F}}^2(t). \tag{13}$$

This gives three main frequency components: a DC signal, a signal at the frequency ν, and a signal at the double frequency 2ν. To measure the Verdet constant, we use the amplitude of the signal at 2ν[15]

$$A_{2\nu} = \frac{\Theta_0^2}{2\sqrt{1 + \left(\frac{2\nu}{\nu_{\mathrm{c}}}\right)^2}}, \tag{14}$$

where $\nu_{\mathrm{c}} = 1/4\pi\tau$ is the cavity cutoff frequency, introduced to take into account the cavity filtering.[19] $A_{2\nu}$ is measured for different magnetic field amplitudes, from 0 to about 50 $\times 10^{-3}$ T. The whole is fitted by $K_V B_{\parallel,0}^2$. The Verdet constant finally depends on the measured experimental parameters as follows:

$$V(T,P) = \sqrt{\frac{K_V}{2}}\frac{\left[1 + (8\pi\tau\nu)^2\right]^{1/4}}{2\tau\Delta^{\mathrm{FSR}}L_B}, \tag{15}$$

where T and P are, respectively, the temperature and pressure of the gas.

C. Measurement and error budget

The A- and B-type uncertainties associated to the measurement of V are detailed in Table I.[15,17] They are given at 1σ (coverage factor $k = 1$). The A-type uncertainty is dominated by the photon lifetime uncertainty. The main contributions to the B-type uncertainty come from the uncertainty of the magnetic length and of the fit constant K_V which includes the B-type uncertainty of the magnetic field and of the photodiodes conversion factor.[17]

We have measured the Verdet constant in xenon at T = (294 ± 1) K and for 5 pressures from 1.01×10^{-3} to 5.01×10^{-3} atm. In this range of pressure, xenon can be considered as an ideal gas and the Verdet constant is thus proportional to

TABLE I. Parameters and their respective relative A- and B-type uncertainties at 1σ that have to be measured to infer the value of the Verdet constant V. Typical values are given at $P = 5\times10^{-3}$ atm.

Parameter	Typical value	Relative A-type uncertainty	Relative B-type uncertainty
τ (ms)	1.14	2.0×10^{-2}	
K_V (rad T^{-1})	1.07	3×10^{-3}	3.2×10^{-2}
Δ^{FSR} (MHz)	65.996		3×10^{-4}
L_B (m)	0.308		1.9×10^{-2}
$V\times10^5$ (rad T^{-1} m^{-1})	1.66	1.8×10^{-2}	2.5×10^{-2}

the pressure. Data are fitted by a linear equation,

$$V(T,P) = V^{\mathrm{n}}P, \tag{16}$$

giving a normalized Verdet constant (P = 1 atm) at λ = 1064 nm and T = (294 ± 1) K,

$$V^{\mathrm{n}} = (3.31\pm0.09)\times10^{-3}\ \mathrm{atm}^{-1}\ \mathrm{rad\ T}^{-1}\ \mathrm{m}^{-1}. \tag{17}$$

The uncertainty is given at 1σ and is detailed in Table II. With a scale law on the gas density, this corresponds to a normalized Verdet constant at T = 273.15 K of

$$V^{\mathrm{N}} = (3.56\pm0.10)\times10^{-3}\ \mathrm{atm}^{-1}\ \mathrm{rad\ T}^{-1}\ \mathrm{m}^{-1}. \tag{18}$$

Using Eq. (2), we can also give the normalized Faraday constant at T = 273.15 K,

$$k_{\mathrm{F}}^{\mathrm{N}} = (1.21\pm0.03)\times10^{-9}\ \mathrm{atm}^{-1}\ \mathrm{T}^{-1}. \tag{19}$$

IV. LINEAR MAGNETIC BIREFRINGENCE

A. Magnetic field

The transverse magnetic field $B_\perp$ is generated by an X-Coil, specially designed by the High Magnetic Field National Laboratory (LNCMI-Toulouse, France) for the measurement of the vacuum magnetic birefringence. This coil has been presented and discussed in great detail in several previous papers.[14,20] Very briefly, the magnet delivers a pulsed magnetic field over an equivalent length L_B of 0.137 m. The total duration of the pulse is about 10 ms with a maximum reached within 2 ms. For the present measurements, a maximum magnetic field of 3 T has been used. Finally, the high-voltage connections can be remotely switched to reverse the direction of the field.

TABLE II. Parameters and their respective relative A- and B-type uncertainties at 1σ that have to be measured to infer the value of the normalized Verdet constant V^{n}. The uncertainty given by the linear fit takes into account the A-type uncertainty of V.

Parameter	Typical value	Relative A-type uncertainty	Relative B-type uncertainty
$V\times10^5$ (rad T^{-1} m^{-1})	1.66	1.8×10^{-2}	2.5×10^{-2}
$P\times10^3$ (atm)	5		2×10^{-3}
Linear fit$\times10^3$ (atm^{-1} rad T^{-1} m^{-1})	3.31	1.5×10^{-2}	
$V^{\mathrm{n}}\times10^3$ (atm^{-1} rad T^{-1} m^{-1})	3.31	1.5×10^{-2}	2.5×10^{-2}

Thus, we can set $\mathbf{B}_\perp$ parallel or antiparallel to the x direction, as shown in Fig. 1.

B. Data analysis

The data analysis follows the one described for the Cotton-Mouton effect measurement in helium.[15] We will, however, detail the main steps, since a slightly different method was used in the present case.

To extract the ellipticity $\Psi_{\mathrm{CM}}(t)$ from Eq. (10), we calculate the following $Y(t)$ function:

$$\begin{aligned} Y(t) &= \frac{\frac{I_{\mathrm{e}}(t)}{I_{\mathrm{t,f}}(t)} - I_{\mathrm{DC}}}{2|\Gamma|} \\ &= \gamma\Psi_{\mathrm{CM}}(t) + \frac{\Psi_{\mathrm{CM}}^2(t)}{2|\Gamma|} + \gamma\frac{|\epsilon|\Theta_{\mathrm{F}}(t)}{2|\Gamma|} + \frac{\Theta_{\mathrm{F}}^2(t)}{2|\Gamma|}, \end{aligned} \tag{20}$$

where γ stands for the sign of Γ. I_{DC} is the static signal measured just before the application of the magnetic field. The absolute value of the static ellipticity $|\Gamma|$ is also measured before each pulse.

Two parameters are adjustable in the experiment: the sign γ of the static ellipticity Γ and the direction of the transverse magnetic field. We acquire signals for both signs of Γ and both directions of $\mathbf{B}_\perp$: parallel to x is denoted as > 0 and antiparallel is denoted as < 0. This gives four data series: ($\Gamma > 0$, $B_\perp > 0$), ($\Gamma > 0$, $B_\perp < 0$), ($\Gamma < 0$, $B_\perp < 0$), and ($\Gamma < 0$, $B_\perp > 0$).

For each series, signals calculated with Eq. (20) are averaged and denoted as $Y_{>>}$, $Y_{><}$, $Y_{<<}$, and $Y_{<>}$. The first subscript corresponds to $\Gamma > 0$ or < 0 while the second one corresponds to $\mathbf{B}_\perp$ parallel or antiparallel to x. This average function can be written in a more general form than the one of Eq. (20). It is the sum of different effects with different symmetries, denoted as s

$$\begin{aligned} Y_{>>} &= +\Psi + \frac{1}{2}\left\langle\frac{1}{\Gamma_{>>}}\right\rangle s_{++} + \left\langle\frac{1}{\Gamma_{>>}}\right\rangle s_{--} + \frac{1}{2}\left\langle\frac{1}{\Gamma_{>>}}\right\rangle s_{+-}, \\ Y_{><} &= +\Psi + \frac{1}{2}\left\langle\frac{1}{\Gamma_{><}}\right\rangle s_{++} + \left\langle\frac{1}{\Gamma_{><}}\right\rangle s_{--} + \frac{1}{2}\left\langle\frac{1}{\Gamma_{><}}\right\rangle s_{+-}, \\ Y_{<<} &= -\Psi + \frac{1}{2}\left\langle\frac{1}{\Gamma_{<<}}\right\rangle s_{++} + \left\langle\frac{1}{\Gamma_{<<}}\right\rangle s_{--} + \frac{1}{2}\left\langle\frac{1}{\Gamma_{<<}}\right\rangle s_{+-}, \\ Y_{<>} &= -\Psi + \frac{1}{2}\left\langle\frac{1}{\Gamma_{<>}}\right\rangle s_{++} + \left\langle\frac{1}{\Gamma_{<>}}\right\rangle s_{--} + \frac{1}{2}\left\langle\frac{1}{\Gamma_{<>}}\right\rangle s_{+-}. \end{aligned} \tag{21}$$

The first subscript in s corresponds to the symmetry with respect to the sign of Γ and the second one to the symmetry with respect to the direction of $\mathbf{B}_\perp$. The subscript + indicates an even parity while the subscript − indicates odd parity. The ratio $\langle 1/\Gamma\rangle$ is the average of $1/|\Gamma|$ measured during corresponding series. The terms Ψ_{CM}^2 and Θ_{F}^2 are included in s_{++}, $\gamma|\epsilon|\Theta_{\mathrm{F}}$ included in s_{--}, and s_{+-} corresponds to a spurious signal with an odd parity towards the direction of $\mathbf{B}_\perp$ and an even parity with respect to the sign of Γ. The ellipticity $\gamma\Psi_{\mathrm{CM}}$ corresponds to s_{-+}.

From this set of four equations with four unknown quantities (Ψ_{CM}, s_{++}, s_{--}, and s_{+-}), we extract $\Psi_{\mathrm{CM}}(t)$, which is fitted by $\alpha B_{\perp,\mathrm{f}}^2$. The cavity filtering should again be taken into account, as indicated by the subscript f.[15,19] The Cotton-Mouton constant k_{CM} finally depends on the measured

TABLE III. Parameters that have to be measured to infer the value of the Cotton-Mouton constant k_{CM} and their respective relative A- and B-type uncertainties at 1σ. Typical values are given at $P = 8\times10^{-3}$ atm.

Parameter	Typical value	Relative A-type uncertainty	Relative B-type uncertainty
τ (ms)	1.14	2.0×10^{-2}	
$\alpha\times10^5$ (T^{-2})	2.82	2.8×10^{-4}	2.2×10^{-2}
Δ^{FSR} (MHz)	65.996		3×10^{-4}
L_B (m)	0.137		2.2×10^{-2}
λ (nm)	1064.0		$<5\times10^{-4}$
$\sin2\theta_P$	1.0000		9×10^{-4}
$k_{CM}\times10^{16}$ (T^{-2})	2.31	2.0×10^{-2}	3.1×10^{-2}

experimental parameters as follows:

$$k_{CM}(T,P) = \frac{\alpha}{4\pi\tau\Delta^{FSR}}\frac{\lambda}{L_B}\frac{1}{\sin 2\theta_P}. \quad (22)$$

C. Measurement and error budget

The A- and B-type uncertainties associated to the measurement of k_{CM} are detailed in Table III and are given at 1σ. The B-type uncertainties have been evaluated previously and detailed in Ref. 17. They essentially come from the length of the magnetic field L_B and the fit constant α.

We have measured the Cotton-Mouton constant in xenon at $T = (293 \pm 1)$ K and for nine pressures ranging from 3 $\times 10^{-3}$ to 8×10^{-3} atm. The data as a function of the pressure are fitted by a linear equation, and we obtain for the value of the Cotton-Mouton constant at $P = 1$ atm,

$$k^n_{CM} = (2.41 \pm 0.37)\times10^{-14}\ T^{-2}\ atm^{-1}. \quad (23)$$

The uncertainty given at 1σ is detailed in Table IV. The dominant uncertainty comes from the linear fit of the Cotton-Mouton constant versus pressure (A-type). The value of k^n_{CM} normalized at 273.15 K is calculated with a scale law on the gas density,

$$k^N_{CM} = (2.59 \pm 0.40)\times10^{-14}\ T^{-2}\ atm^{-1}. \quad (24)$$

V. OUR CALCULATIONS

The Verdet constant and the Cotton-Mouton birefringence were computed within Coupled Cluster response theory,[4,5] at the CCSD[7–9] and CC3[10–13] levels of approximation. Specifically, the Verdet constant was obtained from the following frequency-dependent quadratic response function:[4,21–23]

$$V(\omega) = C\omega\langle\langle\mu_x;\mu_y,L_z\rangle\rangle_{\omega,0}, \quad (25)$$

with $C = \frac{Ne}{8m_e\epsilon_0c_0} = 0.912\,742\times10^{-7}$ in atomic units, N the number density ($N = \frac{P}{k_BT}$ for ideal gases), e the elementary charge, m_e the electron mass, c_0 the speed of light *in vacuo*, $\omega/2\pi$ the frequency of the probing light, and μ_x and L_z are Cartesian components of the electric dipole and angular momentum operators, respectively. The hypermagnetizability anisotropy $\Delta\eta$ entering the Cotton-Mouton birefringence in Eq. (4) (the only term contributing for atoms) is given by the combination of a quadratic and a cubic response functions,[3]

$$\begin{aligned}\Delta\eta &= -\frac{1}{4}\langle\langle\mu_x;\mu_x,L_z,L_z\rangle\rangle_{\omega,\omega,0} - \frac{1}{4}\langle\langle\mu_x;\mu_x,\Theta_{xx}\rangle\rangle_{\omega,0}\\ &\equiv \Delta\eta^p + \Delta\eta^d, \end{aligned} \quad (26)$$

with Θ_{xx} the xx Cartesian component of the traceless quadrupole operator. At the CC3 level, calculations were performed at three different wavelengths, namely, 1064, 632.8, and 514.5 nm. At the CCSD level, we computed the dispersion coefficients, as done in our previous study,[24] i.e., for the Verdet constant,

$$V(2n) = 2nS(-2n-2); \quad (27)$$

$$V(\omega) = C\sum_{n=1}^{\infty}\omega^{2n}V(2n); \quad (28)$$

whereas for the Cotton-Mouton constant,

$$\Delta\eta(2n) = -\frac{1}{4}[(2n+1)(2n+2)S(-2n-4) + B(2n)]; \quad (29)$$

$$\Delta\eta(\omega) = \sum_{n=0}^{\infty}\omega^{2n}\Delta\eta(2n). \quad (30)$$

Above, $S(k)$ is the Cauchy moment,

$$S(k) = \sum_{m\neq0}2\omega_{m0}^{k+1}\langle0\mid\mu_z\mid m\rangle\langle m\mid\mu_z\mid0\rangle, \quad (31)$$

with $\hbar\omega_{m0}$ indicating the excitation energy from the ground state 0 to the excited state(s) m, and $B(2n)$ being the dispersion coefficient introduced when expanding, for frequencies below the lowest excitation energy, the electric dipole–electric dipole–electric quadrupole quadratic response function $B_{x,x,xx}(-\omega;\omega,0) = \langle\langle\mu_x;\mu_x,\Theta_{xx}\rangle\rangle_{\omega,0}$ in a convergent power series in the circular frequency ω,

$$B_{x,x,xx}(-\omega;\omega,0) = \sum_{n=0}^{\infty}\omega^{2n}B(2n). \quad (32)$$

For further details on how the above Cauchy moments and dispersion coefficients of the given quadratic response function are computed within coupled cluster response theory, the reader should refer to Refs. 24–26.

Relativistic effects were approximately accounted for by employing relativistic effective core potentials (ECPs)[27] and specifically pseudo-potentials (PPs). "Small core" effective pseudo-potentials were used to describe the 28 inner electrons (that is, the [Ar]$3d^{10}$ core), whereas the remaining 26 valence

TABLE IV. Parameters and their respective relative A- and B-type uncertainties at 1σ that have to be measured to infer the value of the normalized Cotton-Mouton constant k^n_{CM}.

Parameter	Typical value	Relative A-type uncertainty	Relative B-type uncertainty
$k_{CM}\times10^{16}$ (T^{-2})	2.31	2.0×10^{-2}	3.1×10^{-2}
$P\times10^3$ (atm)	5		2×10^{-3}
Linear fit$\times10^{14}$ (T^{-2} atm^{-1})	2.41	1.5×10^{-1}	
$k^n_{CM}\times10^{14}$ (T^{-2} atm^{-1})	2.41	1.5×10^{-1}	3.1×10^{-2}

TABLE V. Dispersion coefficients of the Verdet and Cotton-Mouton response functions at the CCSD level of theory (atomic units).

n	$B(2n)$	$S(-2n-4)$	$S(-2n-2)$	$V(2n)$	$\Delta\eta(2n)$
			aug_cc_pvqz_pp		
0	−654.894 71	126.505 95			100.470 70
1	−8 903.382 5	763.598 99	126.505 95	253.011 90	−64.951 345
2	−92 298.251	5 369.048 6	763.598 99	3 054.396 0	−17 193.302
3	−860 869.9	41 692.560	5 369.048 6	32 214.292	−368 478.36
4			41 692.560	333 540.48	
			d-aug_cc_pvqz_pp		
0	−739.156 30	126.971 74			121.303 23
1	−9 822.912 7	774.871 90	126.971 74	253.943 48	131.112 47
2	−106 369.19	5 553.232 1	774.871 90	3 099.487 6	−15 056.943
3	−1 074 975.1	44 095.369	5 553.232 1	33 319.393	−348 591.39
4			44 095.369	352 762.95	
			t-aug_cc_pvqz_pp		
0	−748.341 87	126.919 27			123.625 83
1	−9 940.721 8	774.472 34	126.919 27	253.838 54	161.763 43
2	−107 513.63	5 551.377 1	774.472 34	3 097.889 4	−14 756.921
3	−1 084 127.2	44 088.280	5 551.377 1	33 308.263	−346 204.12
4			44 088.280	352 706.24	

electrons were correlated as in standard non-relativistic calculations. The basis sets used were constructed starting from the singly augmented aug_cc_pvxz_pp (x = t,q) sets of Peterson *et al.*[28] Since single augmentation is usually not sufficient to ensure converged results, at least for the Cotton-Mouton birefringence, additional sets of diffuse functions were added by applying an even-tempered generation formula commonly used for this purpose to the orbital functions describing the valence electrons, while retaining the pseudo-potential of the original set. The resulting sets are labeled d-aug and t-aug, for double and triple augmentation, respectively.

Where pseudo-potentials parametrically account for relativistic effects on the innermost orbitals, other relativistic effects (e.g., higher-order and picture change effects, and spin-orbit coupling) could play a significant role.[29,30] When dealing with valence properties like electric hyperpolarizabilities, the higher-order relativistic effects and picture change effects (for the dipole operator and also the electron-electron interaction) are expected to be not so important. Also, spin-orbit coupling should be quite weak. Both the Faraday and Cotton Mouton birefringences, however, involve the magnetic dipole operator. In general, relativistic effects on magnetic properties can be more significant and more difficult in terms of picture change (the operators look different in relativistic and non-relativistic theory, and this may require a correction of the property operator that one uses as a perturbation).[29,30]

Nonetheless, also given that the most stringent requirement in terms of basis set convergence is the inclusion of

TABLE VI. CC3 values of the response function components (in atomic units) involved in the Verdet and Cotton-Mouton birefringences. The Verdet constant $V^{\mathrm{N}}(\omega)$ is given in atm^{-1} rad T^{-1} m^{-1} and the Cotton-Mouton constant $k_{\mathrm{CM}}^{\mathrm{N}}$ is in T^{-2} atm^{-1} at 273.15 K.

λ (nm)	$\langle\langle\mu_x;\mu_y,L_z\rangle\rangle_{\omega,0}$	$V^{\mathrm{N}}(\omega)\times10^3$	$\langle\langle\mu_x;\mu_x,\Theta_{xx}\rangle\rangle_{\omega,0}$	$\langle\langle\mu_x;\mu_x,L_z,L_z\rangle\rangle_{\omega,\omega,0}$	$\Delta\eta$	$k_{\mathrm{CM}}^{\mathrm{N}}\times10^{14}$
			aug_cc_pvqz_pp			
1064	11.1587	3.505	−668.242	272.564	98.9195	2.239
632.8	19.5823	10.35	−700.706	308.069	98.1593	2.222
514.5	24.9438	16.22	−728.260	339.617	97.1607	2.200
			d-aug_cc_pvqz_pp			
1064	11.2155	3.522	−755.936	274.099	120.459	2.727
632.8	19.6927	10.40	−791.994	310.285	120.427	2.726
514.5	25.0963	16.32	−822.705	342.514	120.048	2.718
			t-aug_cc_pvqz_pp			
1064	11.2127	3.521	−765.680	274.031	122.912	2.782
632.8	19.6878	10.40	−802.186	310.210	122.994	2.784
514.5	25.0901	16.31	−833.274	342.435	122.710	2.778

diffuse functions as in the case of the electric hyperpolarisability, it is reasonable to assume that both properties are essentially valence properties, for which picture change effects are typically small, and we reckon therefore that the use of (PP)ECPs can be considered accurate enough.

The results obtained in the x = q basis sets are summarized in Tables V and VI, for CCSD and CC3, respectively.

All calculations were performed with the Dalton code.[31]

VI. RESULTS AND DISCUSSION

A. Faraday effect

1. Experiments

We can compare our value of the normalized Verdet constant to the other published values. The most extensive experimental compilation of Verdet constants has been reported by Ingersoll and Liebenberg in 1956, for several gases including xenon[32] for wavelengths ranging from 363.5 to 987.5 nm, with a total uncertainty of about 1%. These values are plotted in Fig. 2.

No datum has ever been reported for λ = 1064 nm. Nevertheless, we can extrapolate its value from the points of Fig. 2, by fitting the data with a function of form $V = A/\lambda^2 + B/\lambda^4$ (solid curve in Fig. 2).[32,33] A supplementary systematic uncertainty should also be added, since the authors measured the ratio between Faraday effects in xenon and in distilled water and rescaled their measurements with accepted values for water.[32,33] Thus, it does not correspond to absolute measurements of the Faraday effect, contrary to ours.

At λ = 1064 nm and T = 273.15 K, we obtain $V^N = (3.46 \pm 0.04) \times 10^{-3}$ atm^{-1} rad T^{-1} m^{-1}. The 1σ uncertainty includes the one given by the fit. This value is compatible with our experimental value (Eq. (18)), represented as the open circle in Fig. 2 and as the straight and dashed lines in Fig. 3.

2. Theory

We can also compare our experimental value with theoretical predictions (both ours and from the literature), plotted in Fig. 3 and summarized in Table VII at 1 atm, 273.15 K and with the gas number density of an ideal gas. To convert from theoretical results given in atomic units into the units used

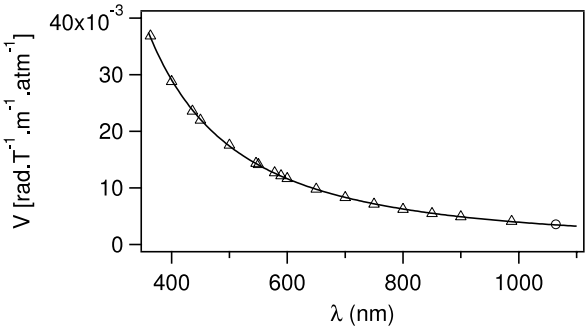

FIG. 2. △: Experimental values of xenon normalized Verdet constant at T = 273.15 K reported by Ingersoll and Liebenberg[32] for wavelengths ranging from 363 nm to 987.5 nm. These values are fitted by the law $A/\lambda^2 + B/\lambda^4$ (solid line). ○: Our experimental value at T = 273.15 K.

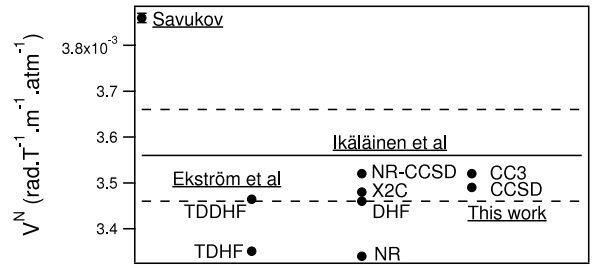

FIG. 3. Normalized Verdet constant of xenon at T = 273.15 K at λ = 1064 m. Solid line: Our experimental mean value. Dashed lines: Our experimental value with 1σ uncertainty. Points: Theoretical predictions (both ours and from the literature). See text and Table VII for the references.

experimentally, we exploited the relation

$$V\ (\text{atm}^{-1}\ \text{rad}\ \text{T}^{-1}\ \text{m}^{-1}) = V\ (\text{a.u.}) \times 8.039\,617 \times 10^4. \tag{33}$$

Our experimental value is compatible within 1σ with our "best" coupled cluster results (t-aug_cc_pvqz_pp basis) and also with the most complete theoretical predictions by Ekström *et al.*[6] and by Ikäläinen *et al.*[34] (see below), and within 3σ with that of Savukov.[35]

The uncertainty of a few percent obtained on our experimental value allows to comment on the agreement with theoretical predictions as a function of the theoretical approximation or model. Savukov[35] has used a relativistic particle-hole configuration interaction (CI) method. He does not give a value at 1064 nm, but the latter can be interpolated, as done with the previous experimental data of Ingersoll and Liebenberg,[32] obtaining the value of Table VII, with an uncertainty given by the fit. The agreement between Savukov's interpolated result and experiment is only within 3σ, even if relativistic effects are taken into account. Ekström *et al.*[6] have used the non-relativistic time-dependent Hartree-Fock (TDHF in Fig. 3) and the relativistic time-dependent Dirac-Hartree-Fock (TDDHF in Fig. 3). There is clearly a better

TABLE VII. Experimental and theoretical values of the normalized Verdet constant at T = 273.15 K, λ = 1064 nm, with uncertainties at 1σ.

References	$V^N \times 10^3$ (atm^{-1} rad T^{-1} m^{-1})	Remarks
Experiment		
Ingersoll *et al.*[32]	3.46 ± 0.04	Interpolated with $A/\lambda^2 + 2B/\lambda^4$. Scaled to water.
This work	3.56 ± 0.10	
Theory		
Savukov[35]	3.86 ± 0.01	Interpolated in this work with $A/\lambda^2 + B/\lambda^4$.
Ekström *et al.*[6]	3.35	TDHF
Ekström *et al.*[6]	3.46	TDDHF
Ikäläinen *et al.*[34]	3.34	NR
Ikäläinen *et al.*[34]	3.48	X2C
Ikäläinen *et al.*[34]	3.46	DHF
Ikäläinen *et al.*[34]	3.52	NR-CCSD
This work	3.49	CCSD/t-aug_cc_pvqz_pp
This work	3.52	CC3/t-aug_cc_pvqz_pp

TABLE VIII. Experimental (uncertainties of 1σ) and theoretical values of the Cotton-Mouton constant of xenon at $T = 273.15$ K.

References	λ (nm)	$k_{CM}^{N} \times 10^{14}$ (T^{-2} atm^{-1})
Experiment		
Carusotto *et al.*[36]	514.5	(2.29 ± 0.10)
Hüttner[37]	632.8	(2.41 ± 0.12)
Bregant *et al.*[38,39]	1064	(3.02 ± 0.27)
This work	1064	(2.59 ± 0.40)
Theory		
Bishop *et al.*[40]	∞	2.665
This work, CCSD/t-aug_cc_pvqz_pp	514.5	2.803
This work, CCSD/t-aug_cc_pvqz_pp	632.8	2.808
This work, CCSD/t-aug_cc_pvqz_pp	1064	2.804
This work, CC3/t-aug_cc_pvqz_pp	514.5	2.778
This work, CC3/t-aug_cc_pvqz_pp	632.8	2.784
This work, CC3/t-aug_cc_pvqz_pp	1064	2.782

agreement (better than 1σ) between their calculations and our experimental value when relativistic effects are taken into account. Finally, Ikäläinen *et al.*[34] have used the non-relativistic Hartree-Fock method (NR in Fig. 3), the exact two-component method (X2C in Fig. 3), and the fully relativistic four-component method (DHF in Fig. 3). The same authors also report (in the supplementary material[34]) a non-relativistic CCSD result (NR-CCSD in Fig. 3). While their uncorrelated results confirm that relativistic effects should be taken into account to improve agreement with experiment, their non-relativistic CCSD result highlights how the inclusion of correlation effects is equally important. Also worth noticing is the rather poor performance of the Becke Lee Yang and Parr (BLYP) and its 3-parameters variant (B3LYP) functionals, which overestimate the value of the Verdet constant in both non-relativistic and relativistic calculations. This also applies for the Becke-Half-and-Half-LYP functional (BHandHLYP) in the relativistic calculations, whereas the non-relativistic BHandHLYP value is still within 1σ of our experimental result (see Table S5 of the supplementary material of Ref. 34).

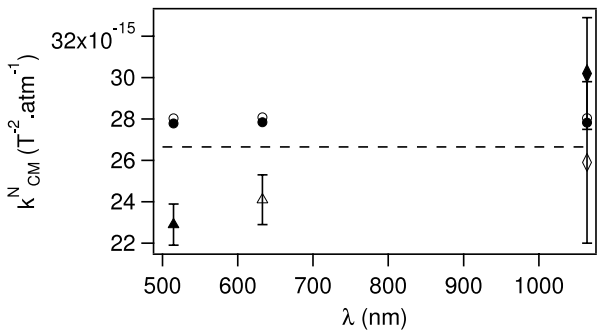

FIG. 4. Reported values of Cotton-Mouton constant of xenon for λ ranging from 514.5 nm to 1064 nm and with 1σ uncertainty. Experimental values: black triangle: Carusotto *et al.*,[36] open triangle: Hüttner (private communication by Bishop *et al.*),[37] black diamond: Bregant *et al.*,[38,39] and open diamond: this work. Theoretical predictions: dashed line: self-consistent-field (SCF) method for λ = ∞ by Bishop,[40] open circle: this work, CCSD, and black circle: this work, CC3.

B. Cotton Mouton effect

1. Experiments

Only a few measurements of the Cotton-Mouton effect in xenon have been discussed in the literature. There is one at λ = 514.5 nm by Carusotto *et al.*,[36] one at λ = 632.8 nm by Hüttner (reported as a private communication by Bishop *et al.*),[37] and finally one at λ = 1064 nm by Bregant *et al.*[38,39] Our experimental value, referring to λ = 1064 nm is compatible within 1σ with the data of Refs. 38 and 39. The set of results is shown in Table VIII and plotted as a function of the wavelength in Fig. 4.

Our measurement has an uncertainty of about 15%. This value, which is larger than that of the other reported values, especially those given for wavelengths of 514.5 nm and 632.8 nm, was established via a complete error budget. Note that no information is available on the setup, the number of pressures, the error budget, and the evaluation of the uncertainty for the value reported at λ = 632.8 nm by Bishop *et al.*[37] as a private communication of Hüttner. The value reported at λ = 514.5 nm by Carusotto *et al.*[36] was measured only at 1 atm, and by comparing the observed magnetic birefringence with that of nitrogen under the same experimental conditions, therefore taking as a reference, assumed as free of uncertainty, the Cotton-Mouton constant of nitrogen. It is safe to say therefore that the uncertainty associated to their datum might be underestimated. Finally, the value reported by Bregant *et al.*[38,39] at λ = 1064 nm corresponds to the weighted average between measurements at two different pressures (9 pressures for our measurement) and the uncertainty is similar to ours.

2. Theory

The Cotton-Mouton constant k_{CM} is linked to $\Delta\eta$ by the relationship[3]

$$k_{CM}\,(\mathrm{atm}^{-1}\,\mathrm{T}^{-2}) = \frac{6.183\,81 \times 10^{-14}}{T}\Delta\eta\ (\mathrm{a.u.}). \quad (34)$$

Only one theoretical prediction has been published so-far for the Cotton-Mouton effect in xenon.[40] The calculation of Bishop and Cybulski was performed at the SCF level of approximation, and it yielded the static hypermagnetizability anisotropy $\Delta\eta$. As stated by the authors, relativistic effects were not taken into account, even though the authors expected them to play a substantial role. Our experimental value agrees with that theoretical prediction within 1σ.

Our computed coupled cluster results, both CCSD and CC3, in the largest (t-aug_cc_pvqz_pp) basis sets for the three wavelengths at which experimental results are available are given in Table VIII. Both the CCSD and CC3 values at 1064 nm are well within 1σ of our experimental measurement, and just within 1σ of the result by Bregant *et al.*[38,39] At 632.8 nm, the agreement of our CC3 value with the experimental result of Hüttner[37] is just outside 3σ. At 514.5 nm, our computed values fall well outside 3σ of the estimate of Carusotto *et al.*[36] This apparently confirms that the error associated to this measured value might be underestimated.

VII. CONCLUSION

We have carried out a thorough analysis of the Faraday (circular) and Cotton Mouton (linear) birefringences of xenon, at a wavelength of 1064 nm. The study involves both an experimental segment, exploiting the capabilities of a state-of-the-art optical setup, and a computational element, where sophisticated wavefunction structure and optical response models (and with an estimate of the effect of relativity) were employed.

Our experimental estimate for the normalized Verdet constant of xenon at a temperature of 273.15 K and $\lambda = 1064$ nm, $V^{\mathrm{N}} = (3.56 \pm 0.10) \times 10^{-3}$ atm^{-1} rad T^{-1} m^{-1}, is very well reproduced by our theoretical approach, which yields a value ($V^{\mathrm{N}} = 3.52 \times 10^{-3}$ atm^{-1} rad T^{-1} m^{-1} using the CC3 approximation) within 1σ of the measured datum.

With respect to the Cotton Mouton effect, at $T = 273.15$ K and $\lambda = 1064$ nm, experiment yields a normalized constant $k^{\mathrm{N}}_{\mathrm{CM}} = (2.59 \pm 0.40) \times 10^{-14}$ atm^{-1} T^{-2}, whereas we compute (again with our most sophisticated model, CC3) a value of $k^{\mathrm{N}}_{\mathrm{CM}} = 2.78 \times 10^{-14}$ atm^{-1} T^{-2}, therefore within 1σ of experiment.

ACKNOWLEDGMENTS

We thank all the members of the BMV collaboration, and in particular J. Béard, J. Billette, P. Frings, B. Griffe, J. Mauchain, M. Nardone, J.-P. Nicolin, and G. Rikken for strong support. We are also indebted to the whole technical staff of LNCMI. Sonia Coriani acknowledges useful discussions with Lucas Visscher and Trond Saue. We acknowledge the support of the *Fondation pour la recherche IXCORE* and the *Agence National de la Recherche* (Grant No. ANR-14-CE32-0006).

[1]L. D. Barron, *Molecular Light Scattering and Optical Activity* (Cambridge University Press, Cambridge, 2004).
[2]A. Rizzo and S. Coriani, "Birefringences: A challenge for both theory and experiment," Adv. Quantum Chem. **50**, 143–184 (2005).
[3]C. Rizzo, A. Rizzo, and D. M. Bishop, "The Cotton-Mouton effect in gases: Experiment and theory," Int. Rev. Phys. Chem. **16**, 81–111 (1997).
[4]T. Helgaker, S. Coriani, P. Jørgensen, K. Kristensen, J. Olsen, and K. Ruud, "Recent advances in wave function-based methods of molecular-property calculations," Chem. Rev. **112**, 543–631 (2012).
[5]O. Christiansen, C. Hättig, and P. Jørgensen, "Response functions from Fourier component variational perturbation theory applied to a time-averaged quasienergy," Int. J. Quantum Chem. **68**, 1–52 (1998).
[6]U. Ekström, P. Norman, and A. Rizzo, "Four-component Hartree–Fock calculations of magnetic-field induced circular birefringence—Faraday effect—in noble gases and dihalogens," J. Chem. Phys. **122**, 074321 (2005).
[7]G. D. Purvis and R. J. Bartlett, "A full coupled cluster singles and doubles model: The inclusion of disconnected triples," J. Chem. Phys. **76**, 1910 (1982).
[8]H. Koch, A. S. de Meras, T. Helgaker, and O. Christiansen, "The integral-direct coupled cluster singles and doubles model," J. Chem. Phys. **104**, 4157 (1996).
[9]C. Hättig, O. Christiansen, H. Koch, and P. Jørgensen, "Frequency-dependent first hyperpolarizabilities using coupled cluster quadratic response theory," Chem. Phys. Lett. **269**, 428 (1997).
[10]H. Koch, O. Christiansen, P. Jørgensen, A. Sanchez de Merás, and T. Helgaker, "The CC3 model: An iterative coupled cluster approach including connected triples," J. Chem. Phys. **106**, 1808 (1997).
[11]O. Christiansen, H. Koch, and P. Jørgensen, "Response functions in the CC3 iterative triple excitation model," J. Chem. Phys. **103**, 7429 (1995).
[12]J. Gauss, O. Christiansen, and J. F. Stanton, "Triple excitation effects in coupled-cluster calculations of frequency-dependent hyperpolarizabilities," Chem. Phys. Lett. **296**, 117 (1998).
[13]F. Pawlowski, "Development and implementation of CC3 response theory for calculation of frequency-dependent molecular properties. Benchmarking of static molecular properties," Ph.D. thesis (Aarhus University, 2004).
[14]R. Battesti, B. Pinto Da Souza, S. Batut, C. Robilliard, G. Bailly, C. Michel, M. Nardone, L. Pinard, O. Portugall, G. Trénec, J.-M. Mackowski, G. L. Rikken, J. Vigué, and C. Rizzo, "The BMV experiment: A novel apparatus to study the propagation of light in a transverse magnetic field," Eur. Phys. J. D **46**, 323–333 (2008).
[15]A. Cadène, D. Sordes, P. Berceau, M. Fouché, R. Battesti, and C. Rizzo, "Faraday and Cotton-Mouton effects of helium at $\lambda = 1064$ nm," Phys. Rev. A **88**, 043815 (2013).
[16]A. Cadène, P. Berceau, M. Fouché, R. Battesti, and C. Rizzo, "Vacuum magnetic linear birefringence using pulsed fields: Status of the BMV experiment," Eur. Phys. J. D **68**, 16 (2014).
[17]P. Berceau, M. Fouché, R. Battesti, and C. Rizzo, "Magnetic linear birefringence measurements using pulsed fields," Phys. Rev. A **85**, 013837 (2012).
[18]R. V. Pound, "Electronic frequency stabilization of microwave oscillators," Rev. Sci. Instrum. **17**, 490–505 (1946).
[19]P. Berceau, M. Fouché, R. Battesti, F. Bielsa, J. Mauchain, and C. Rizzo, "Dynamical behaviour of birefringent Fabry-Pérot cavities," Appl. Phys. B: Lasers Opt. **100**, 803–809 (2010).
[20]S. Batut, J. Mauchain, R. Battesti, C. Robilliard, M. Fouché, and O. Portugall, "A transportable pulsed magnet system for fundamental investigations in quantum electrodynamics and particle physics," IEEE Trans. Appl. Supercond. **18**, 600–603 (2008).
[21]S. Coriani, C. Hättig, P. Jørgensen, A. Halkier, and A. Rizzo, "Coupled cluster calculations of Verdet constants," Chem. Phys. Lett. **281**, 445–451 (1997).
[22]S. Coriani, C. Hättig, P. Jørgensen, A. Halkier, and A. Rizzo, "Erratum: "Coupled cluster calculations of Verdet constants" [Chem. Phys. Lett. **281**, 445 (1997)]," Chem. Phys. Lett. **293**, 324 (1998).
[23]S. Coriani, P. Jørgensen, O. Christiansen, and J. Gauss, "Triple excitation effects in coupled cluster calculations of Verdet constants," Chem. Phys. Lett. **330**, 463–470 (2000).
[24]S. Coriani, C. Hättig, and A. Rizzo, "The electric-field-gradient-induced birefringence of Helium, Neon, Argon, and SF_6," J. Chem. Phys. **111**, 7828–7836 (1999).
[25]C. Hättig, O. Christiansen, and P. Jørgensen, "Cauchy moments and dispersion coefficients using coupled cluster linear response theory," J. Chem. Phys. **107**, 10592 (1997).
[26]C. Hättig and P. Jørgensen, "Dispersion coefficients for first hyperpolarizabilities using coupled cluster quadratic response theory," Theor. Chem. Acc. **100**, 230 (1998).
[27]M. Dolg, "Effective core potentials," in *Modern Methods and Algorithms of Quantum Chemistry*, NIC Series Vol. 1, edited by J. Grotendorst (John von Neumann Institute for Computing, Jülich, 2000), pp. 479–508.
[28]K. Peterson, D. Figgen, E. Goll, H. Stoll, and M. Dolg, "Systematically convergent basis sets with relativistic pseudopotentials. II. Small-core pseudopotentials and correlation consistent basis sets for the post-d group 16-18 elements," J. Chem. Phys. **119**, 11113 (2003).
[29]T. Saue, "Spin-interactions and the non-relativistic limit of electrodynamics," Adv. Quantum Chem. **48**, 383–405 (2005).
[30]T. Saue, "Relativistic Hamiltonians for chemistry: A primer," ChemPhysChem **12**, 3077–3094 (2011).
[31]K. Aidas, C. Angeli, K. L. Bak, V. Bakken, R. Bast, L. Boman, O. Christiansen, R. Cimiraglia, S. Coriani, P. Dahle, E. K. Dalskov, U. Ekström, T. Enevoldsen, J. J. Eriksen, P. Ettenhuber, B. Fernández, L. Ferrighi, H. Fliegl, L. Frediani, K. Hald, A. Halkier, C. Hättig, H. Heiberg, T. Helgaker, A. C. Hennum, H. Hettema, E. Hjertenæs, S. Høst, I.-M. Høyvik, M. F. Iozzi, B. Jansik, H. J. A. Jensen, D. Jonsson, P. Jørgensen, J. Kauczor, S. Kirpekar, T. Kjærgaard, W. Klopper, S. Knecht, R. Kobayashi, H. Koch, J. Kongsted, A. Krapp, K. Kristensen, A. Ligabue, O. B. Lutnæs, J. I. Melo, K. V. Mikkelsen, R. H. Myhre, C. Neiss, C. B. Nielsen, P. Norman, J. Olsen, J. M. H. Olsen, A. Osted, M. J. Packer, F. Pawlowski, T. B. Pedersen, P. F. Provasi, S. Reine, Z. Rinkevicius, T. A. Ruden, K. Ruud, V. Rybkin, P. Salek, C. C. M. Samson, A. S. de Merás, T. Saue, S. P. A. Sauer, B. Schimmelpfennig, K. Sneskov, A. H. Steindal, K. O. Sylvester-Hvid, P. R. Taylor, A. M. Teale, E. I. Tellgren, D. P. Tew, A. J. Thorvaldsen, L. Thøgersen, O. Vahtras, M. A. Watson, D. J. D. Wilson, M. Ziolkowski, and H. Ågren, "The Dalton quantum chemistry program system," WIREs: Comput. Mol. Sci. **4**, 269–284 (2014).

[32]L. R. Ingersoll and D. H. Liebenberg, "Faraday effect in gases and vapors II," J. Opt. Soc. Am. **46**, 538–542 (1956).
[33]L. Rosenfeld, "Zur Theorie des Faradayeffekts," Z. Phys. **57**, 835 (1929).
[34]S. Ikäläinen, P. Lantto, and J. Vaara, "Fully relativistic calculations of Faraday and nuclear spin-induced optical rotation in xenon," J. Chem. Theory Comput. **8**, 91 (2012).
[35]I. M. Savukov, "Particle-hole configuration-interaction polarizabilities and Verdet constants of noble-gas atoms," Phys. Rev. A **85**, 052512 (2012).
[36]S. Carusotto, E. Iacopini, E. Polacco, F. Scuri, G. Stefanini, and E. Zavattini, "Measurement of the magnetic birefringence of noble gases," J. Opt. Soc. Am. B **1**, 635–640 (1984).
[37]D. M. Bishop and J. Pipin, "Hypermagnetizability anisotropy (Cotton-Mouton effect) for the rare gases and methane," Chem. Phys. Lett. **186**, 195–197 (1991).
[38]M. Bregant, G. Cantatore, S. Carusotto, R. Cimino, F. Della Valle, G. Di Domenico, U. Gastaldi, M. Karuza, E. Milotti, E. Polacco, G. Ruoso, E. Zavattini, and G. Zavattini, "Measurement of the Cotton-Mouton effect in krypton and xenon at 1064 nm with the PVLAS apparatus," Chem. Phys. Lett. **392**, 276–280 (2004).
[39]M. Bregant, G. Cantatore, S. Carusotto, R. Cimino, F. Della Valle, G. Di Domenico, U. Gastaldi, M. Karuza, V. Lozza, E. Milotti, E. Polacco, G. Raiteri, G. Ruoso, E. Zavattini, and G. Zavattini, "Erratum: 'Measurement of the Cotton-Mouton effect in krypton and xenon at 1064 nm with the PVLAS apparatus' [Chem. Phys. Lett. **392**, 276 (2004)] and 'A precise measurement of the Cotton-Mouton effect in neon' [Chem. Phys. Lett. **410**, 288 (2005)]," Chem. Phys. Lett. **477**, 415 (2009).
[40]D. M. Bishop and S. M. Cybulski, "Calculation of electromagnetic properties of the noble gases," Chem. Phys. Lett. **211**, 255–258 (1993).